The Coaxial Beam-Rotating Antenna (COBRA): Theory of Operation and Measured Performance

Clifton C. Courtney, *Senior Member, IEEE*, and Carl E. Baum, *Fellow, IEEE*

***Abstract*—Many microwave generators, especially high-power sources, utilize an azimuthally symmetric output mode such as the TM_{01} circular waveguide or the coaxial TEM mode. If such a mode is projected into an antenna aperture and radiated directly, then a doughnut-shaped radiation pattern with a boresight null will result. Antenna designs to directly accommodate an azimuthally symmetric output mode and the high electric fields of high-power sources have been considered, but they tend to be low gain, do not radiate a boresight peak along the axis of the source, and the pattern peak direction changes with frequency. Mode conversion techniques to alter the aperture field distribution (i.e., TM_{01} to TE_{11} in circular waveguide) have also been explored, but losses and weight, size and cost additions impact negatively on total system design. This paper describes a novel antenna we call the coaxial beam-rotating antenna (COBRA) that mitigates many of the problems normally associated with the azimuthally symmetric output modes of high-power microwave sources. The COBRA accepts directly (without the need for mode conversion) an azimuthally symmetric guided mode of a microwave source and radiates a high-gain pattern with a boresight peak. In addition, the COBRA operates with a wide bandwidth, is compatible with the intense electric fields associated with high-power microwave sources, and the geometry of the antenna can be easily configured to produce an arbitrarily (elliptically) polarized boresight field. This paper presents the fundamental theory of operation, derives pertinent design and performance equations, and gives the measured operating characteristics of a COBRA prototype.**

***Index Terms*—Circular waveguide, coaxial transmission line, reflector antennas.**

I. Introduction

MANY conventional and high-power microwave (HPM) electromagnetic sources utilize the TM_{01} circular waveguide or TEM coaxial modes as the output mode. For example, the magnetically insulated line oscillator (MILO) HPM source [1] will initially extract microwave energy in a coaxial geometry, then convert the RF energy from the coaxial TEM mode to a TM_{01} circular waveguide mode. The relativistic klystron oscillator (RKO) uses a similar microwave extraction geometry [2]. If radiated directly, these azimuthally symmetric modes will generate a doughnut-shaped pattern with a null on boresight. Often, mode conversion techniques are used to change the undesirable mode to one that results in a radiation pattern with a boresight peak such as circular TE_{11} or rectangular TE_{01} mode [3]. Unfortunately, mode conversion introduces system losses (conversion efficiencies of between 50 and 75% are typical), and the addition of the mode converter adds weight and length to the system (source, converter, antenna). Other antenna designs like the Vlasov [4] and the shaped end radiator [5], [6] antennas, have been considered to radiate azimuthally symmetric aperture distributions, but they typically radiate a low-gain pattern with an off-boresight peak that changes direction as a function of the frequency (for high-power sources, the frequency tends to shift about a nominal center frequency during the output duty cycle). Consequently, the nature in which the microwave energy is pointed becomes an issue for some high-power applications.

This paper describes a novel concept for an antenna named the coaxial beam-rotating antenna (COBRA) that can accept directly microwave energy in an azimuthally symmetric mode and radiate a high-gain elliptically polarized [7], boresight peak. In addition, the geometry of the COBRA design is compatible with many HPM sources and the scale lengths associated with the antenna can accommodate the intense electric fields that exist in the output region of these sources. Also, the COBRA can project circularly polarized electric fields, which enhance the probability of efficiently coupling microwave energy though apertures of a potential target.

In this paper, it is shown that a standard paraboloidal reflector can be segmented into N sectors and the surface profile adjusted to produce arbitrary elliptical polarization on boresight from a general azimuthally symmetric field excitation. In the following sections, the fundamental concepts of operation are described. Also, governing equations for the surface geometry of the COBRA reflector are determined and the analysis of the radiated field of the COBRA aperture is presented as a function of the number of steps in the main reflector and the excitation field distribution. Also, calculations of the radiated field and the gain of a hypothetical COBRA configuration are given and characteristics of the measured radiated field of a COBRA prototype are presented. In conclusion, a brief overview of different feed architectures for the COBRA geometry is given. The appendix provides several gain definitions used as an antenna performance metric in the analysis presented.

II. Fundamental Concepts of Operation

In this section, the fundamental concepts of the COBRA are explained and it is shown how the geometry of the antenna transforms an azimuthally symmetric mode distribution into an aperture distribution that radiates a circularly polarized field with a boresight peak.

Fig. 1 illustrates a paraboloidal reflector fed by a conical horn antenna. The horn is driven by an azimuthally symmetric mode (such as the TM_{01} mode of circular waveguide), located with

Manuscript received August 12, 1997; revised June 1, 1998. This work was supported by the United States Air Force Research Laboratory, Directed Energy Directorate, under Contracts F29601-96-C-0044 and F29601-97-C-0005.

C. C. Courtney is with Voss Scientific, Albuquerque, NM 87108 USA.

C. E. Baum is with the Air Force Research Laboratory, Directed Energy Directorate, Albuquerque, NM 87117 USA.

Publisher Item Identifier S 0018-926X(00)01271-0.

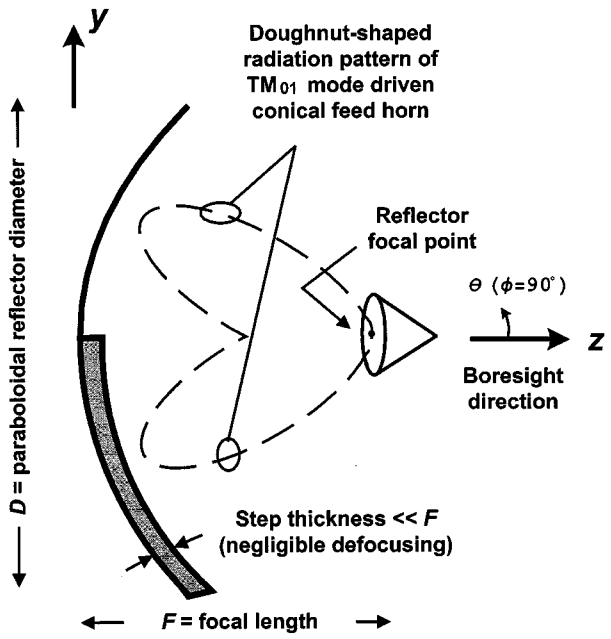

Fig. 1. A cross-sectional view of a paraboloidal reflector illuminated by the radiated field of a TM_{01} mode driven conical horn. The reflector surface can be altered to modify the phase distribution across the aperture.

its phase center at the focal point of the reflector [8]. As depicted in the figure, the conical horn radiates a doughnut-shaped pattern onto the reflecting surface. If the reflector were shaped conventionally then the radiated pattern also would exhibit a doughnut-shaped pattern with a null on boresight. However, the surface of the paraboloidal reflector can be modified to alter the path lengths from the focal point of the reflector to two diametrically opposed locations on the reflector surface to the aperture plane. Consider the geometry depicted in Fig. 2(a). There, the reflector surface is shown "stepped" in a prescribed manner so that the difference in the path lengths FA and FA' introduces the proper phase shift in the azimuthally symmetric incident field to produce in-phase illumination of the aperture plane. Since the phase of the incident field at the two diametrically opposed points differs by 180°, the path length difference should introduce an additional 180° shift in the phase of the ray that follows the longer path. In the next section, derivations are given for equations that describe the reflector profile needed to achieve the desired path length relationships.

A. Surface Geometry of the COBRA Reflector

To achieve the proper relationship between the path lengths, the reflector surface profile can be stepped an amount depending on the location of the reflection point on the surface. This step creates a fractional wavelength path difference for two paths starting at the focal point to diametrically opposed points on the reflector surface to the aperture plane. In support of the above discussion, the path length difference between FA and FA' should be $\lambda/2$ for any two diametrically opposed points. Then, with reference to Fig. 2(b), the one-way path length difference τ

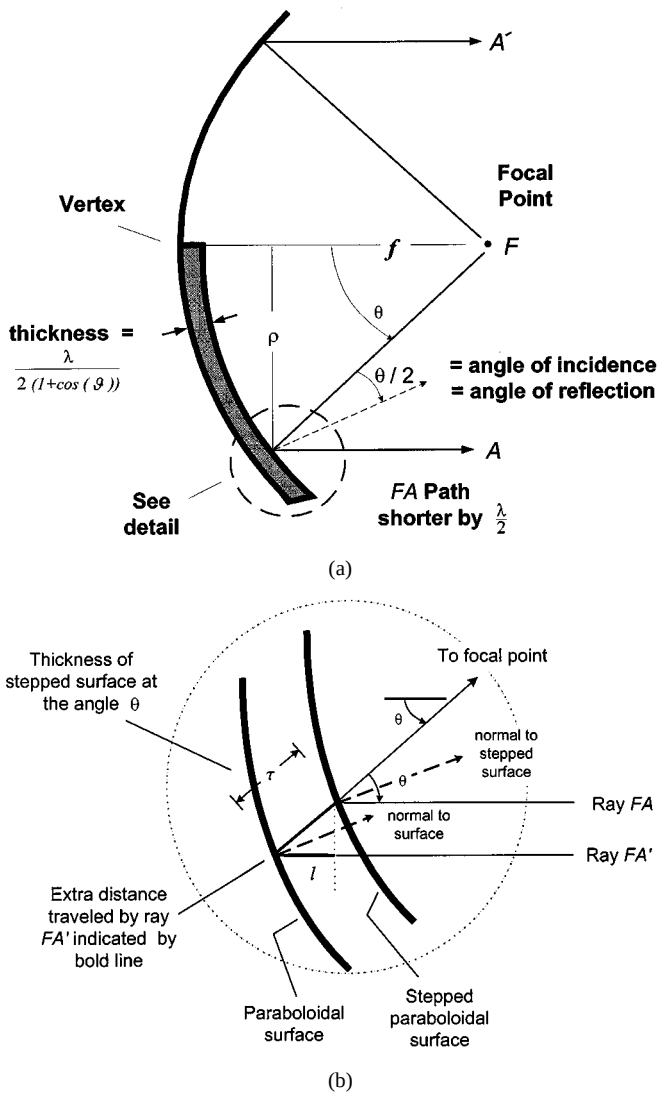

Fig. 2. The surface of the paraboloidal reflector can be modified to produce a path length difference of $\lambda/2$. (a) Location and path length difference of two diametrically opposed points on the surface of the reflector. (b) Detail and closeup of the surface geometry.

can be expressed as $FA - FA' = \tau + l = \lambda/2$ or as a function of the angle θ

$$\tau = \frac{\lambda}{2(1+\cos(\theta))} \tag{1}$$

where θ is the angle from the reflector axis to the point of reflection on the reflector surface.

Equation (1) would be sufficient if the reflector surface were divided into just two sectors. For the case of N sectors, (1) can be generalized as

$$\tau_n(\theta) = \frac{(n-1)\lambda}{N(1+\cos(\theta))} \tag{2}$$

where

$N =$ total number of sectors;

$n =$ specific sector.

Later, it will be shown that the number of equiangular divisions of the reflector affect the properties of the boresight field.

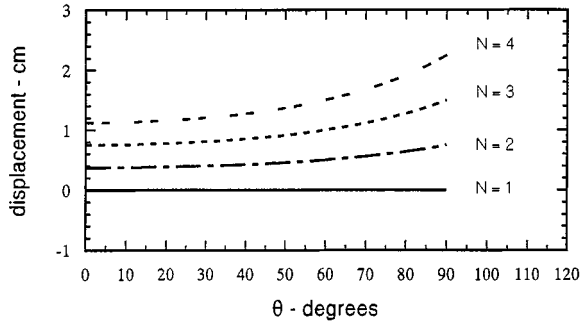

Fig. 3. The displacement of the nominal paraboloidal reflector surface as a function of θ is shown. For this case, the center frequency is 10 GHz and $N = 4$.

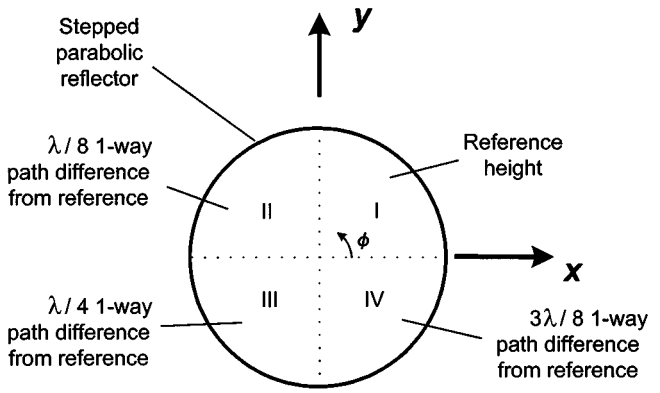

Fig. 4. There are four quadrants associated with the $N = 4$ geometry. The path length from the focal point to the reflector surface to the aperture plane is given by (2), where $n = 1, 2, 3, 4$.

As an example, consider the transformation of a 0.6096-m (24 in)-diameter paraboloidal reflector with a 0.375 F/D ratio into a COBRA reflector with $N = 4$ equiangular steps. With an operating frequency of 10 GHz, the step thickness (displacement) as a function of the angle θ is computed for each sector according to (2) and is shown in Fig. 3. A front-on view of the $N = 4$ COBRA aperture is shown in Fig. 4. Note that the step values are equal to $\lambda/2$ for opposing sectors at $\theta = 0°$ only. This means that a constant translation in the paraboloidal surface of the individual sectors will not yield the proper surface profile. In this example, the focal length is 22.8 cm and the maximum angle is $\theta_{\max} = 67.5°$. Therefore, the maximum step thickness is $\tau_{\max} = 1.627$ cm, which is 7.13% of the focal length. When the maximum step size becomes a substantial percentage of the focal length of the antenna, defocusing of the radiated beam could result. To reduce this effect, a paraboloidal reflector with a higher F/D ratio or longer focal length could be used.

B. The Radiated Field and Aperture Directivity of a COBRA

The function of the steps in the reflector of the COBRA is to transform an azimuthally symmetric incident field into an aperture field that produces a circularly polarized radiated pattern with a boresight peak. It will be shown that $N = 1$ steps is the case of the standard reflector; $N = 2$ generates linear polarization on boresight, just three steps are required to produce circular polarization, and any number of equiangular steps greater than three produces circular polarization on boresight. It will also be shown that the gain of the aperture increases to an asymptotic limit as the number of steps is increased. In the matter of $N \geq 3$, an interesting related phenomenon is discussed in [9], where it is shown that C_N symmetry (N-fold rotation axis) does not depolarize axial scattering. Using the expressions for the radiated field and the definitions for the normalized gain presented here, one can describe the operational characteristics of a COBRA aperture for an arbitrary number of steps in the main or subreflector.

To begin the analysis, the field distribution assumed incident on the reflector is a function of the radial variable (ρ), independent of azimuth (φ) and is oriented in the $\boldsymbol{a}_\rho$ direction (though the analysis holds for a $\boldsymbol{a}_\varphi$ field orientation as well). The assumed electric field distribution incident on the main reflector is then azimuthally symmetric. The excitation field can be written in cylindrical coordinates as $\boldsymbol{E}(\rho, \varphi) = E(\rho)\boldsymbol{a}_\rho$. In Cartesian coordinates the components are $E(\rho)\cos(\varphi)\boldsymbol{a}_x$ and $E(\rho)\sin(\varphi)\boldsymbol{a}_y$. This incident field illuminates the stepped main reflector, which in turn introduces a relative phase shift in the reflected field among the N sectors. Accounting for the path length differences of the sectors of the stepped reflector surface, the projected antenna aperture field can be written as

$$E_x^A = E(\rho)\cos(\varphi)\, e^{j\psi(\varphi)} \tag{3}$$

and

$$E_y^A = E(\rho)\sin(\varphi)\, e^{j\psi(\varphi)}. \tag{4}$$

The phase $\psi(\varphi)$ is dependent on the round-trip distance from the feed horn to the reflector surface and back to the antenna aperture plane; it is a function of the variable φ. This aperture field has been approximated with the following assumptions.

1) The illumination of the reflector is governed by the aperture distribution of the feed horn and is ρ-directed.
2) Feed horn to reflector surface to antenna aperture path length differences modify the phase only.
3) Aperture blockage effects are negligible.
4) Diffraction effects are not important.

Now assume that the reflector has a diameter $D = 2a$ and is stepped in N equal-angle sections. For $2\pi(n-1)/N = \varphi_{n-1} \leq \varphi \leq \varphi_n = 2\pi n/N$, the path length differences produced by stepping the reflector in the manner dictated by (2) produce a phase contribution to the aperture field of

$$\psi(\varphi) = \frac{2\pi(n-1)}{N}, \qquad \text{for } n = 1, 2, \cdots, N. \tag{5}$$

This corresponds to a counterclockwise increase in the step thickness on the reflector. It is later shown that for $N \geq 3$, the counterclockwise (positive z normal to the reflecting surface at the apex) step size increase yields right-hand circular polarization (RHCP), while a clockwise step size increase yields left-hand circular polarization (LHCP). In spherical coordinates, the radiated electric field can be expressed in terms of the electric vector potential [10] as

$$\boldsymbol{E}(\boldsymbol{r}) = j\omega\varepsilon\eta\boldsymbol{a}_r \times \boldsymbol{F}(\boldsymbol{r}) \tag{6}$$

where

$$\boldsymbol{F}(\boldsymbol{r}) = \frac{e^{-jkr}}{4\pi r} \int_{S_A} 2([\boldsymbol{E}^A(\rho', \varphi') \times \hat{\boldsymbol{n}}])\, e^{jk_x x + jk_y y}\, ds' \quad (7)$$

$k_x = k\sin(\vartheta)\cos(\varphi)$, $k_y = k\sin(\vartheta)\sin(\varphi)$, and $\eta = \sqrt{\mu/\varepsilon}$ is the intrinsic wave impedance of the medium. The Cartesian components of the radiated electric vector potential can be computed in terms of the aperture distribution as

$$\begin{aligned} F_x &= \boldsymbol{F}\cdot\boldsymbol{a}_x \\ &= \frac{e^{-jkr}}{4\pi r} \int_{S_A} 2\left([\boldsymbol{E}^A(\rho', \varphi') \times \hat{\boldsymbol{n}}]\cdot\hat{\boldsymbol{a}}_x\right) e^{jk_x x + jk_y y}\, ds' \\ &= \frac{e^{-jkr}}{2\pi r} \int_0^{2\pi}\int_0^a E_y^A(\rho', \varphi')\, e^{jk\rho'\sin\vartheta\cos(\varphi-\varphi')} \\ &\quad \rho'\, d\rho'\, d\varphi \\ &= \frac{e^{-jkr}}{2\pi r} \int_0^{2\pi}\int_0^a E(\rho')\sin(\varphi')\, e^{j\psi(\varphi')} \\ &\quad e^{jk\rho'\sin\vartheta\cos(\varphi-\varphi')}\rho'\, d\rho'\, d\varphi' \end{aligned} \quad (8a)$$

and similarly

$$\begin{aligned} F_y &= \boldsymbol{F}\cdot\boldsymbol{a}_y \\ &= -\frac{e^{-jkr}}{2\pi r} \int_0^{2\pi}\int_0^a E(\rho')\cos(\varphi')\, e^{j\psi(\varphi')} \\ &\quad e^{jk\rho'\sin\vartheta\cos(\varphi-\varphi')}\rho',\, d\rho'\, d\varphi'. \end{aligned} \quad (8b)$$

With the expression for $\psi(\varphi)$given above, the components can be expressed as

$$\begin{aligned} F_x = \frac{e^{-jkr}}{2\pi r} \sum_{n=1}^{N} \exp\left\{j\,\frac{2\pi(n-1)}{N}\right\} \int_{\varphi_{n-1}}^{\varphi_n}\int_0^a E(\rho') \\ \sin(\varphi')\, e^{jk\rho'\sin\vartheta\cos(\varphi-\varphi')}\rho'\, d\rho'\, d\varphi' \end{aligned} \quad (9a)$$

and

$$\begin{aligned} F_y = -\frac{e^{-jkr}}{2\pi r} \sum_{n=1}^{N} \exp\left\{j\,\frac{2\pi(n-1)}{N}\right\} \int_{\varphi_{n-1}}^{\varphi_n}\int_0^a E(\rho') \\ \cos(\varphi')\, e^{jk\rho'\sin\vartheta\cos(\varphi-\varphi')}\rho'\, d\rho'\, d\varphi'. \end{aligned} \quad (9b)$$

When evaluated, the above expressions will yield the complete radiated pattern of the COBRA aperture as a function of the excitation distribution, the number of steps, and the observation angle.

1) COBRA Pattern Boresight Properties: For the case of the boresight direction ($\theta = 0°$, $\phi = 0°$), the above expressions for the potentials can be written as

$$F_x = \frac{e^{-jkr}}{2\pi r} f_E \xi_x(N) \quad (10a)$$

and

$$F_y = -\frac{e^{-jkr}}{2\pi r} f_E \xi_y(N) \quad (10b)$$

where $f_E = 2\pi\int_0^a E(\rho')\rho'\, d\rho'$ contains the radial dependence of the aperture excitation. The terms which contain the azimuthal dependence and that depend on the number of steps N are

$$\xi_x(N) = \frac{1}{2\pi}\sum_{n=1}^{N} e^{j(2\pi(n-1)/N)}(\cos(\varphi_{n-1}) - \cos(\varphi_n)) \quad (11a)$$

and

$$\xi_y(N) = \frac{1}{2\pi}\sum_{n=1}^{N} e^{j(2\pi(n-1)/N)}(\sin(\varphi_n) - \sin(\varphi_{n-1})). \quad (11b)$$

Here we have the important result that due to the azimuthal symmetry of the aperture field, the boresight radiated field factors into terms that separate the radial dependence from the number of steps N. The dependence on N can be factored and evaluated separately, with $\xi_x(N)$ and $\xi_y(N)$ applying to every $E(\rho)$.

The above expressions for $\xi_x(N)$ and $\xi_y(N)$ can be simplified; one writes the $\sin(-)$ and $\cos(-)$ terms as exponentials

$$\begin{aligned} \xi_x(N) = \frac{1}{2\pi}\sum_{n=1}^{N} e^{j(2\pi(n-1)/N)} \\ \left(\frac{e^{j\varphi_{n-1}} + e^{-j\varphi_{n-1}}}{2} - \frac{e^{j\varphi_n} + e^{-j\varphi_n}}{2}\right) \end{aligned} \quad (12)$$

substitutes for φ_{n-1} and φ_n and groups like terms to obtain

$$\begin{aligned} \xi_x(N) = \frac{1}{4\pi}\sum_{n=1}^{N} \left\{\left(1 - e^{-j(2\pi/N)}\right)\right. \\ \left. + \left(e^{-j(4\pi/N)} - e^{-j(2\pi/N)}\right) e^{j(4\pi n/N)}\right\}. \end{aligned} \quad (13)$$

The properties of a finite geometric progression [11, p. 10, eq. 3.1.10] allow reduction to the following forms:

$$\xi_x(N) = \begin{cases} 0, & N = 1 \\ 2/\pi, & N = 2 \\ \xi(N)\, e^{-j\pi(2-N/2N)}, & N \geq 3 \end{cases} \quad (14a)$$

and

$$\xi_y(N) = \begin{cases} 0, & N = 1 \\ 0, & N = 2 \\ \xi(N)\, e^{-j(\pi/N)}, & N \geq 3 \end{cases} \quad (14b)$$

where the magnitude term is

$$\xi(N) = \frac{N}{2\pi}\sin\left(\frac{\pi}{N}\right). \quad (14c)$$

Note that one must evaluate explicitly the first two terms ($N = 1$ and $N = 2$) using (9). Equations (10) and (14) describe the boresight radiated field for the case in which the reflector step thickness increases in the counterclockwise direction. By converting to the time domain, one can show this to be RHCP for all cases where $N \geq 3$. Note that the $N = 1$ case represents an ordinary reflector and produces a null on boresight, while the $N = 2$ case produces a pattern peak with linear polarization on boresight.

To achieve LHCP, one would adjust the reflector surface step distribution such that

$$\psi(\varphi) = 2\pi(1-n)/N$$

for

$$2\pi(1-n)/N = \varphi_{n-1} \le \varphi \le \varphi_n = (-2\pi n/N).$$

This would give a discrete clockwise increase in the step thickness. For this case, it can be shown that

$$\xi_x^{\mathrm{LHCP}}(N) = \begin{cases} 0, & N=1 \\ 2/\pi, & N=2 \\ \xi(N)\, e^{j\pi(2-N/2N)}, & N \ge 3 \end{cases} \tag{15a}$$

and

$$\xi_y^{\mathrm{LHCP}}(N) = \begin{cases} 0, & N=1 \\ 0, & N=2 \\ \xi(N)\, e^{j\pi(1-N/N)}, & N \ge 3. \end{cases} \tag{15b}$$

As before, it is observed that for $N \ge 3$ the components are equal in magnitude and in phase quadrature.

These results can now be used to compute the boresight radiated field characteristics of a COBRA geometry as a function of the number of steps N. For $N = 4$, the far-zone components of the electric vector potential on boresight are

$$\begin{aligned} F_x(N=4) &= f_E \frac{e^{-jkr}}{2\pi r}\xi_x(4) \\ &= f_E \frac{e^{-jkr}}{2\pi r}\left[\frac{1}{\pi}(1-e^{-j(\pi/2)})\right] \end{aligned} \tag{16a}$$

and

$$\begin{aligned} F_y(N=4) &= -f_E \frac{e^{-jkr}}{2\pi r}\xi_y(4) \\ &= -f_E \frac{e^{-jkr}}{2\pi r}\left[\frac{1}{j\pi}(1-e^{-j(\pi/2)})\right] \end{aligned} \tag{16b}$$

where $a = D/2$ is the radius of the aperture. The boresight radiated field then is

$$\begin{aligned} \boldsymbol{E}(r) &= -j\omega\varepsilon\eta \boldsymbol{F}(r) \times \boldsymbol{a}_z = -j\omega\varepsilon\eta[\boldsymbol{a}_x(F_y) - \boldsymbol{a}_y(F_x)] \\ &= -j\omega\varepsilon\eta f_E \frac{e^{-jkr}}{2\pi r}\left(\frac{1-e^{-j(\pi/2)}}{\pi}\right) \\ &\quad \left[\boldsymbol{a}_x\left(\frac{1}{j}\right) + \boldsymbol{a}_y(1)\right] \\ &= j\frac{\sqrt{2}}{\pi} f_E \frac{e^{-j(kr+(\pi/4))}}{\lambda r}[\boldsymbol{a}_x + j\boldsymbol{a}_y]. \end{aligned} \tag{17}$$

Equation (17) describes a circularly polarized field [7] and is characteristic of the boresight field for any azimuthally symmetric aperture distribution. The next sections consider the resulting radiated field of a COBRA for specific aperture distributions.

TABLE I
NORMALIZED BORESIGHT DIRECTIVITY OF A REFLECTOR DRIVEN BY A UNIFORM AZIMUTHALLY SYMMETRIC MODE AS A FUNCTION OF THE NUMBER OF STEPS N

N	$d_L(N)$ in dB	$d_C(N)$ in dB	Comment
1	-∞	-∞	Standard reflector gives boresight null
2	-3.92	-3.92	One step gives linear polarization
3	-7.67	-4.66	First case of circular polarization
4	-6.93	-3.92	Circular polarization
8	-6.25	-3.23	Circular polarization
16	-6.08	-3.07	Circular polarization
32	-6.03	-3.02	Circular polarization
∞	-6.02	-3.01	Asymptotic directivity

2) COBRA Pattern Properties of a Uniformly Filled Aperture: If we assume that the aperture is uniformly illuminated, $\boldsymbol{E}(\rho, \varphi) = E_0 \boldsymbol{a}_\rho$, then the above expressions can be simplified considerably and properties of the boresight gain and polarization of the COBRA can be determined as a function of the number of steps N. For that case, the integrals are easily evaluated and the potential components written as

$$F_x = f_E \frac{e^{-jkr}}{2\pi r}\,\xi_x(N) = (\pi a^2)E_0 \frac{e^{-jkr}}{2\pi r}\,\xi_x(N) \tag{18a}$$

and

$$F_y = -f_E \frac{e^{-jkr}}{2\pi r}\,\xi_y(N) = -(\pi a^2)E_0 \frac{e^{-jkr}}{2\pi r}\,\xi_y(N). \tag{18b}$$

Drawing on the definitions given in the Appendix, the normalized linear directivity (ratio of the directivity of the boresight power density in a single polarization to that of a uniformly filled linearly polarized aperture) of the four-step reflector is $d_L(N=4) = \xi^2(4) = 0.203$, which, in decibels, is $d_L(N=4) = -6.93$ dB. The circularly polarized directivity (ratio of the total boresight radiated power density directivity of the aperture to that of a uniformly filled linearly polarized aperture) is $d_C(4) = 2\xi^2(4) = 0.405$ or $d_C(4) = -3.922$ dB.

The normalized directivity for a uniformly filled azimuthally symmetric aperture distribution can also be computed for an arbitrary number of reflector steps. Table I gives the boresight normalized linear and circular directivities for several values of N.

The case $N = 1$ is that of the standard reflector (with no steps), and the indicated directivity means it radiates a boresight null. For $N = 2$, the aperture radiates linear polarization with a boresight directivity of $d_L = -3.92$ dB. The first incidence of circular polarization occurs for $N = 3$ and the aperture produces circular polarization for all $N \ge 3$. The circular directivity (d_C) is always 3 dB higher than the linear directivity and means that the total power density in the circularly polarized wave is twice that of each linear polarization. As $N \to \infty$ (the case of a smoothly varying reflector surface profile with a single discontinuity) the normalized directivities approach asymptotic limits of $d_C \to -3.01$ dB as $N \to \infty$ and $d_L \to -6.021$ dB as $N \to \infty$.

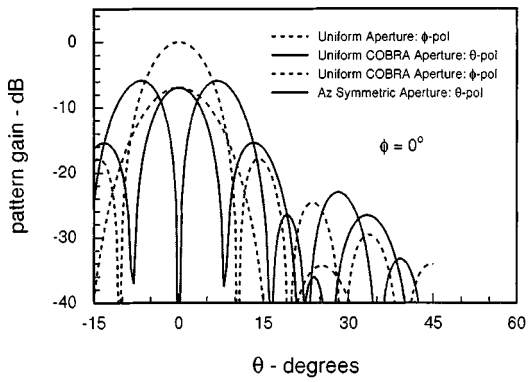

Fig. 5. The computed far-field patterns of three uniformly filled circular apertures are shown. The nonzero radiated fields are shown for the case where the aperture polarization is linear (x-directed), the aperture polarization is azimuthally symmetric ($\boldsymbol{E}(\rho, \varphi) = E_0\boldsymbol{a}_\rho$), and the aperture is filled with an azimuthally symmetric distribution—but modified by an $N = 4$ COBRA aperture (aperture diameter $= 1$ m, frequency $= 1$ GHz).

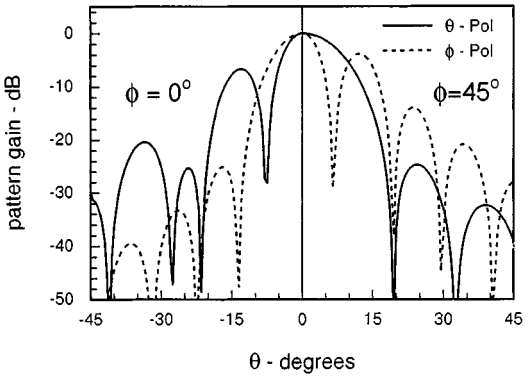

Fig. 6. The computed far-field pattern of an $N = 4$ COBRA circular aperture filled with the TM_{01} circular waveguide mode is shown. The patterns for the θ and ϕ polarizations for $\phi = 0^\circ$ are shown plotted against $-45^\circ \le \theta \le 0^\circ$, and for $\phi = 45^\circ$ are shown plotted against $0^\circ \le \theta \le 45^\circ$ (aperture diameter $= 1$ m, frequency $= 1$ GHz).

The computed far-field patterns of three uniformly filled circular apertures are shown in Fig. 5 for $-15^\circ \le \theta \le 45^\circ$. The nonzero radiated fields are shown for the case where the aperture polarization is azimuthally symmetric ($\boldsymbol{E}(\rho, \varphi) = E_0\boldsymbol{a}_\rho$), the aperture is filled with an azimuthally symmetric distribution but modified by an $N = 4$ COBRA aperture, and the case where the aperture is filled with a linear (x-directed) polarization. The characteristic boresight ($\theta = 0°$) null is apparent for the azimuthally symmetric aperture field, but the null is transformed into a boresight peak (with circular polarization) for the azimuthally symmetric aperture distribution modified by a $N = 4$ COBRA geometry. The pattern for a uniformly filled, x-polarized, circular aperture is also shown in the graph. Note that, as predicted, the peak pattern gain of the linearly polarized pattern is slightly more than 6 dB above each component of the circularly polarized components of the COBRA modified aperture. The computations were made for the case where the aperture diameter $= 1$ m and the frequency $= 1$ GHz.

Though the above results were derived for a uniformly filled aperture, the predicted polarization and gain dependence on the number of steps is applicable to the case of a general azimuthally symmetric excitation.

3) COBRA Pattern Properties of an Aperture Excited with the TM_{01} Circular Waveguide Mode: Let the excitation be supplied by the TM_{01} circular waveguide mode, then the aperture field is proportional to $\boldsymbol{E}(\rho, \varphi) = E_0 J_1(x_{01}\rho/a)\boldsymbol{a}_\rho$, and the resulting vector potentials are given by

$$F_x = E_0 \frac{e^{-jkr}}{2\pi r} \sum_{n=1}^{N} e^{j(2\pi(n-1)/N)} \int_{\varphi_{n-1}}^{\varphi_n} \int_0^a \sin(\varphi') J_1\left(\frac{x_{01}\rho'}{a}\right) e^{jk\rho' \sin\vartheta \cos(\varphi-\varphi')} \rho'\, d\rho'\, d\varphi' \quad (19a)$$

and

$$F_y = E_0 \frac{e^{-jkr}}{2\pi r} \sum_{n=1}^{N} e^{j(2\pi(n-1)/N)} \int_{\varphi_{n-1}}^{\varphi_n} \int_0^a \cos(\varphi') J_1\left(\frac{x_{01}\rho'}{a}\right) e^{jk\rho' \sin\vartheta \cos(\varphi-\varphi')} \rho'\, d\rho'\, d\varphi' \quad (19b)$$

where

$J_1(\cdot)$ Bessel function of the first kind of order 1;

a radius of the main reflector;

x_{01} 2.405.

The computed far-field pattern of an $N = 4$ COBRA circular aperture filled with the TM_{01} circular waveguide mode is shown in Fig. 6. The patterns for the θ and ϕ polarizations for $\phi = 0°$ are shown plotted against $-45° \le \theta \le 0°$, and for $\phi = 45°$ are shown plotted against $0° \le \theta \le 45°$ (aperture diameter $= 1$ m, frequency $= 1$ GHz).

The plots reveal several interesting aspects of the radiated field of the COBRA. First, as predicted each component of the TM_{01} mode-illuminated COBRA aperture is equal in amplitude on boresight and it can be shown that the phase difference between the orthogonal components is 90°. There are differences in the main beam and sidelobe characteristics of the two polarizations. Along the $\phi = 0°$ cut, the ϕ-component of the far field has a narrow main beam with a high sidelobe level relative to the ϕ-component. These relations are reversed for the pattern along the $\phi = 45°$ as shown in the figure. Additionally, it can be shown that the TM_{01} mode-illuminated COBRA aperture with $N = 4$ exhibits a boresight gain that is 1.19 dB below that of a uniformly illuminated, azimuthally symmetric, $N = 4$ COBRA aperture. To compute the pattern for other azimuthally symmetric excitations (the TEM coaxial or conical transmission line modes, for example) one substitutes the form of the mode distribution in (9a) and (9b) and computes the resulting expressions as a function of the angular dependence.

III. Mechanical Characteristics and Measured Performance of a COBRA Prototype

A COBRA prototype was built to verify the radiated characteristics predicted by the analysis. This section describes its physical and mechanical characteristics. Also, the measured antenna performance of the prototype in terms of the absolute pattern gain are presented for a several values of N (the number of sectors of the main reflector).

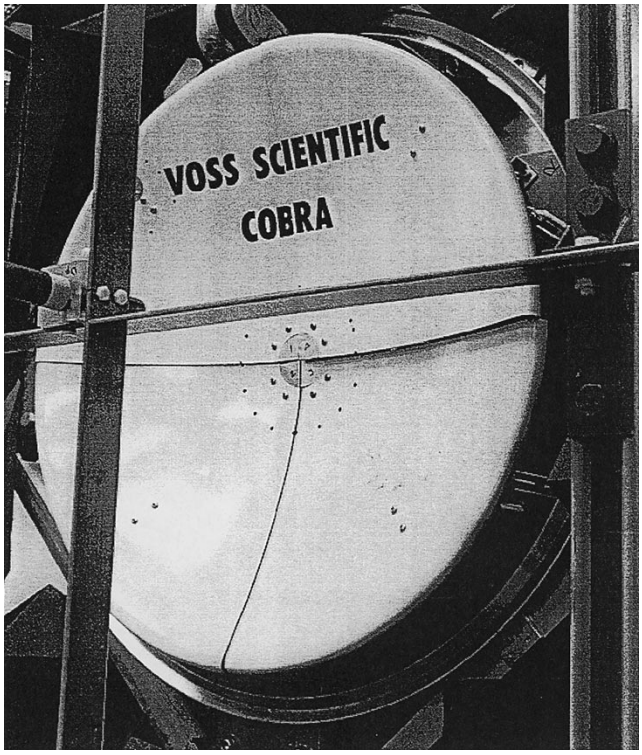

Fig. 7. Photograph of the COBRA prototype is shown. The surface is divided into four equiangular sectors, each with independent translation and rotation.

A. Physical Characteristics of the COBRA Prototype

A prototype antenna was fabricated to demonstrate the properties of the COBRA design and the design equations. Fig. 7 is a front-perspective photograph of the COBRA prototype. It is an $N = 4$ sector design, meaning that the main paraboloidal reflector has been cut into four equal-angle sectors. The sectors are adjustable such that the antenna configuration can be $N = 1, 2,$ or 4. A segmented paraboloidal reflector (diameter $= 0.6096$ m $= 24$ in), with an F/d ratio of 0.375 (focal length $= 22.8$ cm $= 9$ in) comprises the main reflector of the COBRA prototype. The base of the supporting infrastructure is made of 1/4-in aluminum (Al) stock sheet, to which Unistrut elements are attached. These hold and support the antenna's individual quadrants. Two additional Al plates (3/8-in stock) are used for mounting, translational adjustment, and alignment. Three pins (1/2-in diameter) per quadrant are pressed into the lower Al plate, then passed through bushings in the upper plate. A 7/8-in stud is screwed into the bottom plate and provides vertical (translational) adjustment of the quadrant's position with the pins. The four quadrants come together at the reflector's vertex. On the reverse side, a tongue-in-groove geometry mates with an assembly bolted to each quadrant. Turnbuckles, two per quadrant, then permit rotational adjustment. Each turnbuckle has both left- and right-hand thread so rotation in one direction expands the turnbuckle and rotation in the other direction draws it in. The COBRA prototype weighs an estimated 100 kg, and occupies a rectangular volume of approximately 94 cm $\times$ 94 cm $\times$ 76 cm (0.673 m^3).

The feed horn is also visible in Fig. 7. It is simply a circular waveguide (copper pipe, approx. 2.7-cm ID) driven from one end by a coaxial-to-TM$_{01}$ mode launcher, and open at the other.

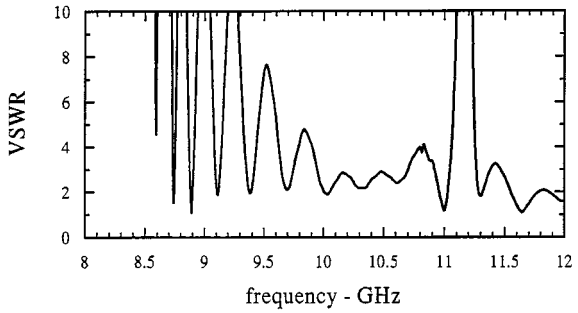

Fig. 8. Input VSWR (as a function of frequency) of the COBRA prototype feed horn. The feed horn was tuned nominally to 10 GHz.

The feed horn is held in place by a Plexiglas housing that permits in /out adjustment. This provides a way to match the horn's phase center to the reflector's focal point. The Plexiglas housing is bolted to a pair of thin fiberglass cross members. These cross members are slotted at the ends and attached to the Unistrut frame. The slots permit x/y adjustment of the location of the feed horn. A mode filter is resident in the circular waveguide and helps prevent propagation to the feed horn aperture of unwanted modes that are not azimuthally symmetric. Each of the four surface quadrants seen in Fig. 7 are positioned in a manner dictated by (2). Because the prototype was built with four independently adjustable surfaces, it can be configured first as an $N = 1$ (nominal configuration) antenna and then as $N = 2$ and $N = 4$ COBRA configurations.

B. Measured Antenna Properties of the COBRA Prototype

The antenna radiation characteristics of the COBRA prototype were measured with an HP 8510C Vector Network Analyzer-based system that was paired with a custom s-parameter test set. The system measures the absolute gain of an antenna under test (AUT) using the comparison method [12]. The next section reports the measured operating characteristics of the feed horn (input impedance and gain pattern), and the COBRA prototype for the cases $N = 1$, $N = 2$, and $N = 4$ (gain pattern and boresight phase relationships). Pattern measurements were made by sweeping the θ-plane ($\phi = 0$ and $\phi = \pi/2$) about boresight (collinear with the z-axis). For these scan orientations, the vertical polarization is the y-component on boresight, and the horizontal polarization is x-component on boresight (see the coordinate system of Fig. 1).

1) Circular Waveguide Feed Properties: The circular waveguide feed horn was excited through a coaxial-to-TM$_{01}$ mode launcher. In order to determine the absolute gain of the system (ignoring ohmic losses) the input impedance or VSWR and the amount of power loss due to impedance mismatch must be determined. The power loss due to impedance mismatch is given by

$$\text{loss} = 10 \log(1 - |s_{11}|^2). \tag{20}$$

The input VSWR of the feed horn was measured and the values as a function of frequency are shown in Fig. 8. The impedance match is seen to be nominally acceptable at the center frequency (10 GHz), where VSWR $= 2:1$, and the associated mismatch power loss is -0.5587 dB. However, the match is much worse

TABLE II
SUMMARY OF THE POWER LOSS VALUES OF THE COBRA PROTOTYPE FEED HORN DUE TO MISMATCH AS A FUNCTION OF FREQUENCY

frequency (GHz)	Loss (dB)
9	-6.67
9.5	-3.75
10	-0.5587
10.5	-1.141
11	-0.025

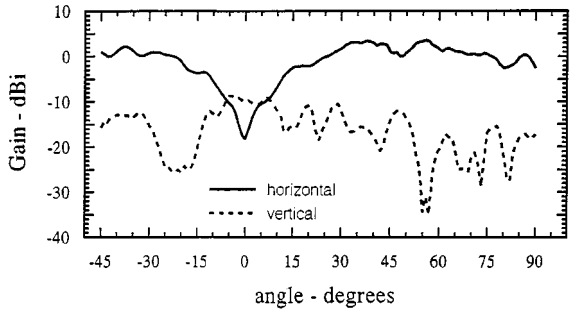

Fig. 9. Measured radiated pattern of the COBRA prototype feed horn for $-\pi/4 \leq \theta \leq \pi/2$ and $\phi = 0$. Both the horizontally and vertically polarized patterns are shown. The pattern was measured at 10 GHz.

at the low end of the frequency band, where the VSWR $> 10:1$ at 9 GHz, and the power loss due to impedance mismatch is -6.67 dB. The power loss due to impedance mismatch must be accounted for in the gain calculations of the COBRA prototype. Table II presents a summary of the power loss due to mismatch in the feed horn for selected frequencies across the band of interest. These values are used to compensate the measured values of gain for the mismatch loss.

The feed horn was removed from its mount at the focal point of the reflector and its pattern was measured for $-\pi/4 \leq \theta \leq \pi/2$ and $\phi = 0$. The measured patterns of the far-field components are shown in Fig. 9. The boresight null associated with the horizontal polarization, due to azimuthally symmetric pattern of the TM_{01} aperture mode of the feed horn, is clearly indicated. The gain of the sidelobes is approximately 3 dBi (=gain relative to isotropic), and the null beam width (angular separation between the -3 dB points of the peaks) is approximately 50°. The ripples in the pattern can be attributed to diffraction off of the horn rim (noticeable since the horn is small electrically and its gain is moderate) and unwanted scattering and chamber reflections. The pattern of the vertically polarized component is also shown in Fig. 9. Due to the symmetry of the field in the aperture, this polarization should be a null across the range of the scan.

2) $N = 1$ COBRA Measurements: The feed horn was remounted at the COBRA prototype's focal point and the reflector surface was adjusted to an $N = 1$ configuration (no offset given to any sector). The horizontally polarized component of the radiated field was measured at 10 GHz for $-\pi/4 \leq \theta \leq \pi/2$ and $\phi = 0$, with 1° steps. The pattern is shown in Fig. 10. The characteristic doughnut pattern and boresight null are clearly indicated. The peak pattern gain is seen to be approximately 25 dBi,

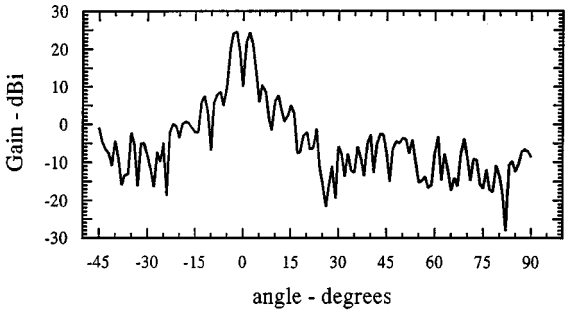

Fig. 10. Measured pattern ($-\pi/4 \leq \theta \leq \pi/2$ and $\phi = 0$) of the horizontally polarized field of the $N = 1$ COBRA prototype at 10 GHz.

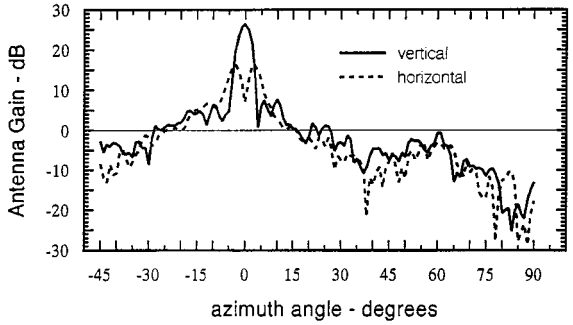

Fig. 11. Measured pattern ($-\pi/4 \leq \theta \leq \pi/2$ and $\phi = 0$) of the horizontally and vertically polarized radiated field of the $N = 2$ COBRA prototype at 10 GHz.

and the null beam width is about 4°. The first sidelobes come in at about 7–10 dBi.

3) $N = 2$ COBRA Measurements: The surface contour of the reflector was next adjusted, according to (2), to realize an $N = 2$ configuration. In this configuration, sectors I and II stayed at their nominal positions (no movement), while sectors III and IV were displaced equally. With the reflector sectors now offset from one another, there is no fixed vertex and the distance from the original vertex to the feed horn aperture was fixed as follows. The mean displacement of each vertex is $\overline{d} = (0 + 0.75)/2 = 0.375$ cm. The original focal length then was added to this value, and the feed horn aperture was placed this distance from the vertex farthest from the feed horn. For the $N = 2$ case, the feed horn was located $25.1 + 0.375 = 25.475$ cm from the vertex of sector I.

According to the theory described earlier for an $N = 2$ configuration, a boresight peak will be achieved for one of the linear polarizations, while the second polarization will continue to exhibit a boresight null. The measured patterns at 10 GHz for $-\pi/4 \leq \theta \leq \pi/2$ and $\phi = 0$ for the vertical and horizontal polarizations are shown in Fig. 11. The doughnut pattern, with a boresight null and maximum pattern gain of 16.5 dBi, is apparent for the horizontally polarized component. The vertical polarization exhibits a boresight peak with a maximum gain of 27 dBi.

A second pattern of the $N = 2$ configuration was measured in the elevation plane ($-\pi/12 \leq \theta \leq \pi/12$ and $\phi = \pi/2$). Fig. 12 shows the measured pattern of the vertical component. The maximum pattern gain is 26.2 dBi, but the pattern now exhibits large sidelobe levels that were not observed in the pattern of Fig. 11.

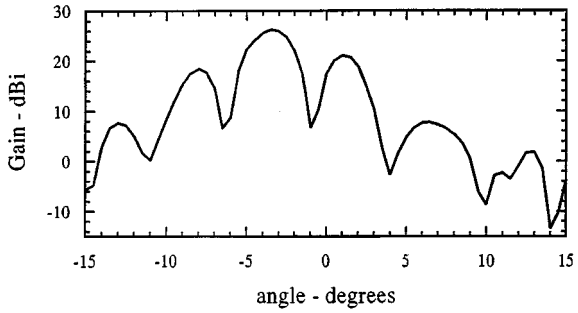

Fig. 12. Measured pattern ($-\pi/12 \leq \theta \leq \pi/12$ and $\phi = \pi/2$) of the vertically polarized radiated field of the $N = 2$ COBRA prototype in the elevation plane. The measurement frequency was 10 GHz.

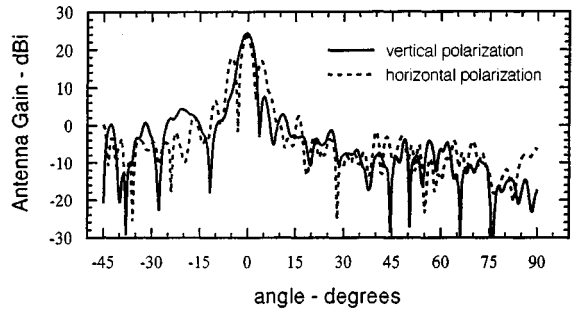

Fig. 13. Measured pattern ($-\pi/4 \leq \theta \leq \pi/2$ and $\phi = 0$) of the horizontally and vertically polarized radiated field of the $N = 4$ COBRA prototype are shown. The measurement frequency was 10 GHz.

Here, the sidelobe levels are about 19 and 21 dBi—much higher than observed in the other principal plane (6 dBi). This increase in the sidelobe levels from one principal plane to the other—the peak-to-sidelobe level ratio is just 5 dB—was also observed in the $N = 4$ measurements. This pattern characteristic was predicted by the analysis of Section II, and it can be shown that the radiated component in the direction that crosses the major discontinuity in the aperture surface will exhibit the high sidelobe level.

4) $N = 4$ COBRA Measurements: The surface contour of the reflector of the prototype was adjusted according to (2) to realize an $N = 4$ configuration with a 10 GHz center frequency. The distance from the feed horn aperture to the main reflector's vertex was fixed as follows: the mean displacement of each vertex (of each sector) was determined as before, in this case $\overline{d} = (0 + 0.375 + 0.750 + 1.124)/4 = 0.562$ cm. The nominal focal length then was added to this value, and the feed horn aperture was placed this distance from the vertex of the paraboloidal sector that remained fixed (at its nominal $N = 1$ position).

The theory described earlier predicts that circular polarization on boresight is achieved for $N = 3$ and all higher N-values. Then the patterns for both polarizations (horizontal and vertical) should exhibit boresight peaks with the same peak value. The patterns of the horizontally polarized and vertically polarized patterns for the $N = 4$ configuration are shown in Fig. 13. The pattern peaks (23.5 and 23.1 dBi) for both polarizations are achieved on boresight, but are down from the $N = 2$ pattern peak (26.8 dBi). Both are predicted in the theory, but note that again large sidelobe levels for one of the polarizations are observed. The peak-to-sidelobe ratios are approximately 5 and 20 dB (the same as observed for the $N = 2$ case).

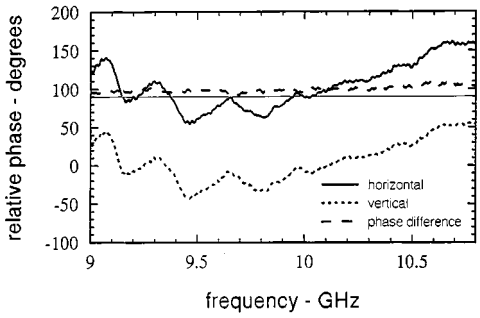

Fig. 14. Relative phase of the two orthogonal components of the boresight field of the $N = 4$ COBRA as a function of frequency. The phase difference is also shown in the graph.

5) $N = 4$ Boresight Phase Relations: Measurements of the patterns of both polarizations for the $N = 4$ configuration have shown that their peak boresight gains are approximately equal. This is consistent with the predicted circularly polarized nature of the boresight field of the $N = 4$ configuration; however, it is not a sufficient condition for circular polarization. Depending on the reference, the phase relationship between the two polarizations should be $\pm 90°$. One polarization should lead or lag the other polarization by 90° (to yield right- or left-handed circular polarization). Fig. 14 gives the measured phase (relative) variation as a function of frequency of the vertical and horizontal polarization components of the boresight field. The absolute phase difference between the two polarizations is simply the difference between the two relative measurements at a particular frequency. The phase difference between the two polarizations is also shown in Fig. 14. One notes that the phase difference at the center frequency (10 GHz) is about 90° (exactly 95.17°).

IV. Conclusion

This paper has presented the fundamental concepts of an antenna we call the coaxial beam-rotating antenna, or COBRA, because it produces a radiated field that exhibits a boresight peak with circular polarization when illuminated by an azimuthally symmetric incident field. Governing design and performance equations were derived, and the physical and mechanical aspects of an X-band prototype were described. An extensive data set of measurements of the radiated field of the prototype COBRA were also presented. The measured data, indicative of the nature of the radiated field for several configurations, supports the analysis and discussion given.

A number of other types of geometries are under investigation. These include: 1) COBRA geometries that utilize subreflectors in Cassegrain and Gregorian configurations [13]; 2) subreflectors driven with the bare or dielectric-coated center conductor of a coaxial transmission line [14]; 3) the use of dielectric-coated reflectors to create the desired path length profile without physically cutting the reflector; and 4) the use of dielectric lenses to condition the azimuthally symmetric field of a horn antenna to radiate circular polarization directly. More complete discussions of the theoretical development [15] and the prototype measurements [16] are available.

APPENDIX
DIRECTIVITY OF LINEARLY AND CIRCULARLY POLARIZED APERTURES

This appendix provides several useful directivity definitions used to measure the performance of the COBRA as a function of the number of steps in the main reflector and to compare the ability of the COBRA to project a total power density (the scalar sum of the power density in each orthogonal polarization) with that of a linearly polarized aperture.

The radiated far field of a linearly polarized, uniformly filled aperture is chosen as the standard by which the COBRA aperture is measured. Let the field

$$E_y^A \boldsymbol{a}_y = E_0 \boldsymbol{a}_y \tag{A.1}$$

uniformly fill a circular aperture of radius a. The boresight radiated electric vector potential is then

$$F_y^U = E_0(\pi a^2)\,\frac{e^{-jkr}}{2\pi r} = E_0\left(D_U\,\frac{\lambda^2}{4\pi}\right)\,\frac{e^{-jkr}}{2\pi r} \tag{A.2}$$

where the directivity of the uniformly filled aperture is well known to be

$$D_U = \frac{4\pi A}{\lambda^2} = \frac{4\pi(\pi a^2)}{\lambda^2}. \tag{A.3}$$

It has been shown that the radiated field of the COBRA aperture exhibits elliptical polarization, with circular polarization being a special case. When referenced to the radiated field of a uniformly filled aperture, one can choose to weigh the ratio of power density in one of the linear components of the circularly polarized field or compare the total power that is the sum of the powers in each polarization. The following definitions are made:

$$D_L = \text{absolute linear directivity of the COBRA aperture.} \tag{A.4}$$

For example, referenced to the x-component of the boresight field, the directivity is

$$D_L = \frac{1}{2}\,\frac{|E_x(R)|^2}{\eta}\,\left(\frac{4\pi R^2}{P^{\mathrm{Rad}}}\right) \tag{A.5}$$

where $P^{\mathrm{Rad}} =$ total radiated power. Also

$$D_C = \text{directivity of the COBRA aperture based on total power density.} \tag{A.6}$$

Then

$$D_C = \frac{1}{2}\,\frac{|E_x(R)|^2 + |E_y(R)|^2}{\eta}\,\left(\frac{4\pi R^2}{P^{\mathrm{Rad}}}\right) \tag{A.7}$$

where $P^{\mathrm{Rad}} = 1/2(E_0^2/\eta)$ is the total radiated power of the aperture. These values can be normalized to the directivity of a uniformly filled aperture; the normalized directivity figures of merit are defined to be

$$d_L = \frac{D_L}{D_U} = \xi^2(N) \tag{A.8}$$

and

$$d_C = \frac{D_c}{D_U} = 2\xi^2(N) \tag{A.9}$$

for $N \geq 3$ on boresight. The last relations are found simply by forming the ratios indicated, then substitution and reduction to simplest form.

REFERENCES

[1] R. Lemke, S. Calico, and M. Clark, "Investigation of a load-limited, magnetically insulated transmission line oscillator (MILO)," *IEEE Trans. Plasma Sci.*, vol. 25, pp. 364–374, Apr. 1997.

[2] K. J. Hendricks *et al.*, "Increasing the RF energy per pulse of an RKO," *IEEE Trans. Plasma Sci.*, vol. 26, pp. 320–325, June 1998.

[3] R. A. Koslover, C. D. Cremer, W. P. Geren, D. E. Voss, and L. M. Miner, "Compact, broadband, high power circular TM01 to TE11 mode converter," U.S. Patent 4 999 591.

[4] S. N. Vlasov and I. M. Orlova, "Quasi-optical transformer which transforms the waves in a waveguide having circular cross-section into a highly directional wave beam," *Radiophys. Quantum Electron.*, vol. 17, pp. 115–119, 1975.

[5] E. Baca *et al.*, "Computational and experimental investigations of shaped end radiators," in *AMEREM'96*, Albuquerque, NM, 1996.

[6] J. H. Beggs, R. J. Luebber, and B. G. Ruth, "Analysis of electromagnetic radiation from shaped-end radiators using the finite-difference time domain method," *IEEE Trans. Antennas Propagat.*, vol. 41, p. 1324, Sept. 1993.

[7] 10 017*IEEE Standard Definitions of Terms for Radio Wave Propagation*, IEEE Std 211-1977.

[8] A. D. Olver, P. J. B. Clarricoats, A. A. Kishk, and L. Shafai, *Microwave Horns and Feeds*, ser. IEEE Electromagn. Waves Ser. 39. New York: IEEE Press, 1994.

[9] C. E. Baum and H. N. Kritikos, "Symmetry in electromagnetics," in *Electromagnetic Symmetry*, C. E. Baum and H. Kritikos, Eds. Washington, DC: Taylor and Francis, 1995, ch. 1.

[10] W. Stutzman and G. Thiele, *Antenna Theory and Design*. New York: Wiley, 1981.

[11] M. Abramowitz and I. Stegun, *Handbook of Mathematical Functions*. New York: Dover, 1965, p. 10.

[12] 10 017*IEEE Standard Test Procedures for Antennas*, ANSI/IEEE Std 149-1979, 1979.

[13] C. C. Courtney *et al.*, "Design and measurement of a Cassegrain-type coaxial beam-rotating antenna," *Sensor and Simulation Note 427*, Nov. 1998.

[14] C. C. Courtney and C. E. Baum, "Design and optimization of a conical transmission-line feed for a coaxial beam-rotating antenna," *Sensor and Simulation Note 429*, Dec. 1998.

[15] ——, "Coaxial beam-rotating antenna (COBRA) concepts," *Sensor and Simulation Note 395*, Apr. 1996.

[16] C. C. Courtney, D. Slemp, D. Baum, C. E. Baum, R. Torres, and W. Prather, "Coaxial beam-rotating antenna (COBRA) prototype measurements," *Sensor and Simulation Note 408*, July 1997.

Clifton C. Courtney (S'84–M'92–SM'99) was born in Bitburg, Germany, on August 29, 1956. He received the B.S. and M.S. degrees in electrical and computer engineering from the University of South Carolina, Columbia, in 1980 and 1984, respectively, and the Ph.D. degree in electrical engineering from Clemson University, Clemson, SC, in 1992.

Since 1992, he has been a Senior Scientist with Voss Scientific, Albuquerque, NM, where his research interests are in the areas of material characterization, antenna design and development, and microwave imaging. He was previously an Antenna Design Engineer with Shakespeare EFD (Newberry, SC), an Electromagnetic Compatibility Engineer with General Electric (Daytona Beach, FL), and an Engineer with the IIT Research Institute (Annapolis, MD), where he developed RF propagation models.

Dr. Courtney is a member of the Antennas and Propagation Society (AP-S), Microwave Theory and Techniques Society (MTT-S), Instrumentation and Measurement Society (IM-S), and Electromagnetic Compatibility Society (EMC-S) of the IEEE. He also is a member of the Tau Beta Pi National Engineering Honor Society. He is now serving his third term as Chairman of the combined Albuquerque Chapter of the IEEE AP-S, MTT, Electromagnetic Compatibility (EMC), and Nuclear and Plasma Sciences after serving three terms as the chapter's treasurer.

Carl E. Baum (S'62–M'63–SM'78–F'84) was born in Binghampton, NY, on February 6, 1940. He received the B.S. (honors), M.S., and Ph.D. degrees in electrical engineering from the California Institute of Technology, Pasadena, in 1962, 1963, and 1969, respectively.

From 1963 to 1967, he was stationed at the Air Force Research Laboratory, Directed Energy Directorate (formerly Phillips Laboratory, formerly Air Force Weapons Laboratory), Kirtland AFB, Albuquerque, NM, and again from 1968 to 1971. Since 1971 he has served as a civil servant with a position as Senior Scientist at the Air Force Research Laboratory. He is editor of several interagency note series on electromagnetic pulse (EMP) and related subjects. He has published four books: *Transient Lens Synthesis: Differential Geometry in Electromagnetic Theory*; *Electromagnetic Symmetry*; *Ultra-Wideband, Short-Pulse Electromagnetics 3*; and *Detection and Identification of Visually Obscured Targets*.

Dr. Baum was awarded the Air Force Research and Development Award (1970), the AFSC Harold Brown Award (1990), and Phillips Laboratory Fellow (1996). He has received the Richard R. Stoddart Award of the IEEE EMC Society (1984). He is the recipient of the 1987 IEEE Harry Diamond Memorial Award with a citation "for outstanding contributions to the knowledge of transient phenomena in electromagnetics." He is a member of Commissions A, B, and E of the U.S. National Committee of the International Union of Radio Science (URSI). He is founder and president of the SUMMA Foundation, which sponsors various electromagnetics related activities including scientific conferences, publications, short courses, fellowships, and awards. He has led an EMP short course and high-power electromagnetics workshops at numerous locations around the globe.